Current Research in Green and Sustainable Chemistry 10 (2025) 100455

Contents lists available at ScienceDirect

Current Research in Green and Sustainable Chemistry

journal homepage: www.elsevier.com/journals/current-research-in-green-and-sustainable-chemistry/2666-0865

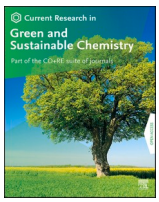

Microwave-assisted synthesis of ZSM-5 from blast furnace slag

Nhlanhla Nyembe [a,b,*], Yusuf M. Isa [a]

[a] Fuel and Petrochemical Synthesis (FPS) Research Group, School of Chemical and Metallurgical Engineering, University of the Witwatersrand, Private Bag 3, Johannesburg, 2050, South Africa

[b] Green Innovations to Fuel Transformation (GIFT) Research Group, Department of Chemical and Metallurgical Engineering, Vaal University of Technology, Andries Potgieter BLVD, Vanderbijlpark, 1911, South Africa

ARTICLE INFO

Keywords:
Blast furnace slag
Crystallinity
Hydrothermal synthesis
Mesoporosity
Microwave irradiation
ZSM-5

ABSTRACT

A rapid hydrothermal synthesis method was employed to prepare a novel Zeolite Socony Mobil-5 (ZSM-5) material impregnated with intrinsic metal alloys (Fe_2O_3, MnO, TiO_2, Cr_2O_3, and NiO). Green chemistry was paired with the synthesis method as a sustainable approach to valorize blast furnace slag (BFS) while addressing the growing demand for high-performance zeolites. This study investigated the role of acid-leached BFS as a precursor and explored the advantages of microwave-assisted hydrothermal synthesis over conventional methods. The synthesis temperature and time were varied to explore their effects on the physicochemical, textural, and structural properties of the synthesized ZSM-5 products, with commercial ZSM-5 serving as a reference material for comparison. The favourable synthesis conditions were found to be 180 °C and 13 h, yielding a crystalline ZSM-5 product characterized by well-defined cubic prism shapes with microsized intergrown rectangular crystals. Furthermore, the synthesized ZSM-5 had a mesoporous structure with an average crystallinity of 52.4 % and a low specific surface area (108.4 m^2/g) compared to the reference sample (436.4 m^2/g). The use of microwave irradiation significantly reduced the synthesis time and energy consumption while preserving the structural integrity of the zeolite framework. Moreover, the synthesis temperature strongly affected the crystal size, while the synthesis time affected the morphology. However, neither the synthesis temperature nor the synthesis time affected the chemical composition of the products. This study highlighted the potential of BFS as a low-cost, sustainable feedstock for zeolite synthesis and the effectiveness of microwave-assisted methods in improving process efficiency. Further work has been proposed to evaluate the potential use of the synthesized ZSM-5 in industrial applications such as catalysis or adsorption processes.

1. Introduction

Zeolite Socony Mobil-5 (ZSM-5) is one of the most sought-after synthetic zeolites that belongs to the Mobil Five (MFI) crystalline structural group and is widely used as a petrochemical catalyst to promote reactions such as alkylation, isomerization, and oligomerization [1]. The three-dimensional crystalline framework in ZSM-5 consists of Si and Al atoms that are tetrahedrally coordinated to form 8-membered and 10-membered rings. The rings are interconnected to form channels and pores. The centrally located atoms (Si and Al) are surrounded by and connected through their shared oxygen atoms, resulting in balanced (SiO_4) and imbalanced (AlO_4^-) ions. The net negative charge is compensated by introducing an extra cation (Na^+, Mg^{2+}, Ca^{2+}, K^+, or H^+) into the tetrahedral units (AlO_4^-). The physicochemical properties that make ZSM-5 attractive to industrialists are its cation exchange capacity (CEC), chemical composition, pore diameter, and channel length [2]. Zeolites are ranked from low-silica zeolites (Si/Al < 2) to high-silica zeolites (Si/Al > 5), and the ranking is based on the Si/Al molar ratio. ZSM-5 is considered a high-silica zeolite, and its chemical composition is used to manipulate properties such as hydrophobicity, thermal stability, catalytic reactivity, and acid resistivity [3]. The uniform pore sizes and long channels found in ZSM-5 contribute to its catalytic activity and shape selectivity, thus enabling it to target compounds of specific shapes and sizes to be adsorbed or catalytically transformed. Regrettably, the narrow micropores (0.5 nm–0.6 nm) prohibit bulky organic molecules from diffusing into the channels to access the active acidic sites, leading to coke formation, reduced catalytic activity, and catalyst deactivation [4]. Attempts to address these drawbacks involved modifying the

* Corresponding author. Fuel and Petrochemical Synthesis (FPS) Research Group, School of Chemical and Metallurgical Engineering, University of the Witwatersrand, Private Bag 3, Johannesburg, 2050, South Africa.
E-mail address: 474649@students.wits.ac.za (N. Nyembe).

https://doi.org/10.1016/j.crgsc.2025.100455
Received 30 January 2025; Received in revised form 9 April 2025; Accepted 19 April 2025
Available online 19 April 2025

synthesis procedure, incorporating strategies such as metal doping, or creating larger pores (mesopores).

ZSM-5 is commonly synthesized using the conventional hydrothermal synthesis method, which involves heat treatment of an aluminosilicate gel in alkaline media under harsh and costly conditions (elevated temperature and pressure). The gel mixture often consists of alumina and silica precursors, an alkali activator, and a structure-directing agent (SDA). Several studies have noted the lack of green chemistry in the hydrothermal synthesis method. Furthermore, the method has been criticized for the feedstock used, harsh synthesis conditions, extensive energy requirements, and prolonged reaction periods. A structure-directing agent (organic template) aims to achieve the desired pore size and framework topology. However, the SDA is often organic and is removed by heat treatment, which releases harmful gasses [5]. Parnham and Morris [6] noted safety concerns that might arise due to the high autogenous pressure that develops during nucleation and crystallization. Moreover, the efficiency of the hydrothermal synthesis method is reduced by operating at elevated temperatures (80–200 °C) for extended periods (1–24 days). This significantly increases the energy requirements of the process [7]. Recent zeolite synthesis studies have focused on addressing the shortfalls in the hydrothermal synthesis process. These include but are not limited to replacing the organic template (SDA) with a seed-assisted synthesis method [8], avoiding autogenous pressure by using the solvent-free synthesis route [9], and using aluminosilicate-rich industrial wastes as feedstock [2]. ZSM-5 produced through these green synthesis methods has been reported to exhibit enhanced crystallinity, improved textural properties, and increased catalytic reactivity. Furthermore, green synthesis methods have significantly reduced the synthesis time, produced less harmful gasses, and decreased energy requirements.

The use of blast furnace slag (BFS) as a silicon and aluminum precursor has been reported as a promising technique for coupling green chemistry with the hydrothermal synthesis method [7]. This is due to the fact that blast furnace slag is a waste byproduct generated by the iron- and steel-making industry and mainly consists of SiO_2 and Al_2O_3 along with impurities (CaO and MgO). Using BFS as a source of SiO_2 and Al_2O_3 could make the synthesis method innovative and environmentally friendly while reducing overall costs. However, the slag's fluctuating mineral and chemical composition significantly affect the leaching efficiency, precursor preparation, and ultimately, the purity and crystallinity of the final product (zeolite). Additionally, the impurities may influence nucleation and crystal growth dynamics, potentially leading to non-uniform zeolite structures or undesired secondary phases. Therefore, beneficiation of BFS mitigates the presence of impurities, and this is achieved by pretreatment of the slag through acid leaching [19]. An alternative method to enhance the environmental sustainability of the hydrothermal synthesis process is the utilization of microwave radiation as an energy source. Microwave energy is an efficient heating method due to the heating mechanisms used. That is, an alternating magnetic and electric field is propagated, and penetrates the sample, thus heating it from the inside out [11]. The benefits of using the microwave-assisted synthesis method are the enhancement of reaction rates, reproducibility of the radiation field, and high product yield and purity [12]. Furthermore, microwave energy accelerates the nucleation of the initial crystals, resulting in the rapid and consistent growth of the crystals. This leads to a product (ZSM-5) with uniform textural properties (pore size and channels) and versatile composition [Si/Al ratio] [7].

Therefore, this communication seeks to enhance the microwave-assisted hydrothermal synthesis method by coupling it with green chemistry processes. This was achieved by employing the microwave-assisted hydrothermal synthesis method to produce a novel ZSM-5 zeolite impregnated with intrinsic metal alloys (Fe_2O_3, MnO, TiO_2, Cr_2O_3, and NiO). Furthermore, blast furnace slag, a waste material from the iron- and steel-making industry, was used as an aluminosilicate precursor. The secondary use of waste slag has the advantages of waste valorization and resource management. The BFS was initially beneficiated using acid leaching to extract Ca and Mg from the slag. While numerous studies have utilized BFS for the preparation of zeolites, the majority rely on conventional hydrothermal synthesis methods. However, this study developed a novel gel preparation method to produce a ZSM-5 material characterized by its crystalline structure and homogeneous properties, providing new insights into the challenges and opportunities of using industrial waste as a precursor. A laboratory-scale microwave system was used to supply microwave energy to control the nucleation and crystallization processes during synthesis. Furthermore, the synthesis conditions, such as the synthesis time and temperature, were investigated systematically. The synthesized ZSM-5 was characterized to determine its structural properties and morphology.

2. Materials and methods

2.1. Chemicals and materials

Blast furnace slag, used as a model industrial waste, was obtained from the iron and steel-making industry in South Africa. The reagents used for the preparation of the synthesis gel were tetrapropylammonium bromide (TPABr, 98 % purity), sodium hydroxide pellets (NaOH, 98 % purity), and sulfuric acid (H_2SO_4, 98 % purity). Hydrochloric acid (HCl, 32 % purity) beneficiated the raw slag. Commercial ZSM-5 (99.5 % purity) was used as the reference zeolite. The chemicals and materials used in this study were obtained from local South African suppliers and used as received. Deionized water was used to prepare all the solutions and was obtained from a Milli-Q® water purification system.

2.2. Blast furnace slag beneficiation

Acid leaching was employed as a pretreatment step to remove impurities (CaO and MgO) and make the slag more suitable for zeolite synthesis. The raw slag was crushed, milled, and screened to a fine particle size passing through a 100 μm sieve and represented as BFS. The prepared BFS was acid-leached using a 3 M HCl solution at 60 °C for 90 min. Subsequently, the leached material was separated from the leachate by gravity filtration, thoroughly washed with deionized water to neutralize residual acid, air-dried for two days, and ground into a fine powder to produce pretreated slag (PTS). A detailed description of the pretreatment process, as well as the characterization of the raw and pretreated slags, is available in Nyembe & Isa [13]. The pretreated slag was used as an aluminosilicate precursor for the synthesis experiments.

2.3. Microwave-assisted hydrothermal synthesis

The conversion of PTS to zeolite ZSM-5 was achieved using a microwave-assisted hydrothermal synthesis technique (Fig. 1), that is, microwave irradiation was used to crystallize the synthesis gel. Calculated amounts of PTS and NaOH were dispersed in deionized water to form suspension 1. Concurrently, TPABr was dissolved in deionized water to form solution 2. Both mixtures were individually stirred and heated to achieve homogeneity. Subsequently, solution 2 was slowly added to suspension 1 while heating and stirring continued for 30 min. The pH level of the resulting mixture was adjusted to 9.0 using H_2SO_4, and a gel mixture was obtained using the following chemical composition:

$$\mathbf{21.7SiO_2 : 4.52Al_2O_3 : 0.75Na_2O : 1.00TPABr : 2225.38H_2O}$$

The gel mixture was then transferred into modified Teflon reaction vessels with a maximum capacity of 50 mL. Each reaction vessel, characterized by its cylindrical shape, operates under a maximum pressure and temperature of 45 bar and 310 °C, respectively. These vessels are constructed from a superior grade, high-density copolymerized material, incorporating SmartVent technology for effective overpressure management, which is activated at thresholds of 20 bar and 250 °C. The reaction vessels were then placed inside the microwave cavity and

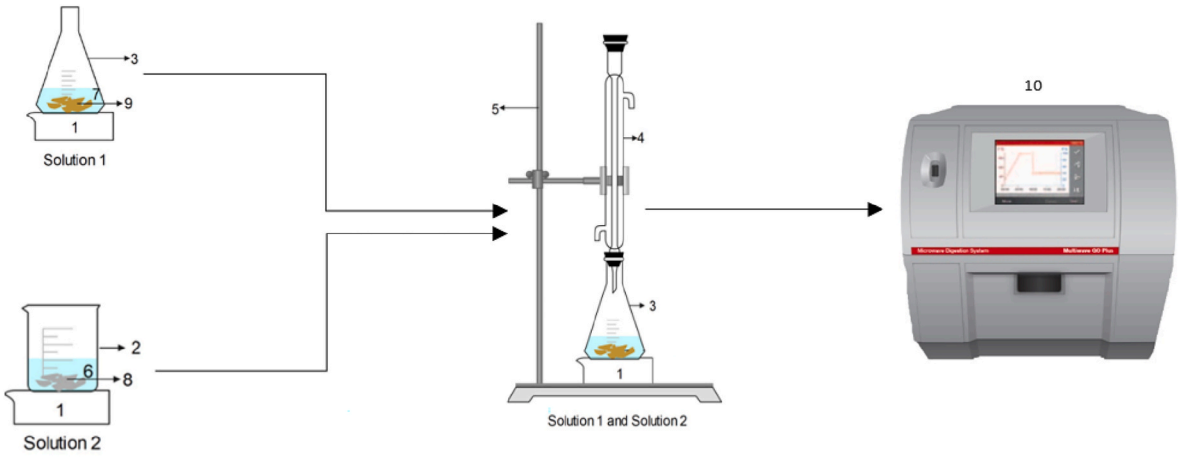

Fig. 1. Hydrothermal synthesis process. 1) heating-magnetic stirring plate, 2) glass beaker, 3) flat-bottomed flask, 4) Liebig glass condenser, 5) clamp stand, 6) deionized water, 7) deionized water and NaOH solution, 8) TPABr, 9) pretreated slag, and 10) microwave system.

heated, using microwave irradiation, to 90 °C, 120 °C, 150 °C, 180 °C and 200 °C and the heating was performed for 5, 7, 9, 11, and 13 h under autogenous pressure. After crystallization, the products were filtered, washed to a neutral pH level, and oven-dried at 90 °C for 24 h. The resulting solids were calcined at 550 °C for 5 h to remove the structure-directing agent (TPABr) and produce Na-ZSM-5.

2.4. Characterization methods

An X-ray fluorescence (XRF) was used to determine the chemical compositions of all the powered samples (BFS, PTS, synthesized ZSM-5, and commercial ZSM-5). The Norrish Fusion technique and an X-ray spectrometer were used to analyze at 50 kV and 50 mA. Major elements were fused using the Johnson Matthey Spectrolflux from 105 to 1000 °C, and the raw data were corrected using in-house software. The powdered samples' X-ray diffraction (XRD) patterns were obtained using a Bruker D2 Phaser powder X-ray analyzer. The instrument consisted of CuK_{α} tubes ($\lambda = 1.5418$ Å), and the data was recorded at a 2θ working range of 5–90° at 40 kV. The step increment was maintained at 0.026°/2θ and a counting time of 0.2 s per step. Semi-quantitative analysis of the powders was performed using custom software, which quantified the mineral phases in each sample. The sample's microstructures (morphology and size) were observed using a high-resolution Tescan Vega scanning electron microscope (SEM). During the analysis, the working distance was maintained between 10 and 15 mm, and the accelerating voltage was set to 5 kV. All samples were coated with carbon and Au/Pd before imaging. Fourier transform infrared spectroscopy (FT-IR) measurements were conducted using a PerkinElmer spectrometer at room temperature after background correction. The sample was placed on the ATR diamond crystal and secured by setting the force gauge to 60 (arbitrary units). It ensured good contact between the diamond crystal and the sample. The infrared spectra were recorded in the 400–4000 cm^{-1} region with a resolution of 4 cm^{-1}.

The textural and structural properties (pore size, specific surface area, and pore volume) of all powdered samples were determined from N_2 adsorption/desorption isotherms collected at −196 °C using a Quantachrome Autosorb iQ3 instrument (Anton Paar, USA). The samples were degassed under vacuum for 3 h at 300 °C. The Brunauer-Emmett-Teller (BET) theory calculates the specific surface area (S_{BET}). The micropore volume (V_{micro}) was determined by using the *t*-plot method. The total pore volume (V_{tot}) was computed at a relative pressure (p/p_0) of 0.98. The adsorption branch of isotherms was used to derive the Barrett-Joyner-Halenda (BJH) model, which was applied to evaluate the mesopore size distributions. With the assumption that commercial ZSM-5 has 100 % crystallinity, the relative crystallinity of the synthesized ZSM-5 was determined using the Integration Method Analysis, as described by Gu et al. [14]. The integration method employs a linear background baseline to assess the sum of the intensities of the characteristic ZSM-5 diffraction peaks (e.g., at 7.6–8.2° and 22.8–24.5° 2θ) with those of the reference commercial ZSM-5 sample, utilizing the following equation.

$$\text{Relative crystallinity } (\%) = \left[\frac{\sum \text{Area of peak intensities (sample)}}{\sum \text{Area of peak intensities (reference)}}\right] \times 100\% \quad (1)$$

3. Results and discussion

3.1. Slag beneficiation

The chemical compositions of BFS and PTS are presented as oxides in Table 1. The main components found in BFS were SiO_2 (40.98 wt%), Al_2O_3 (14.51 wt%), MgO (8.57 wt%), and CaO (29.15 wt%). These reflect the dominant metals in waste slag generated by the iron- and steel-making industry. Acid leaching of the BFS effectively reduced the concentration of impurities (MgO and CaO). However, a significant amount of Al_2O_3 was equally removed. The concentrations of CaO, MgO, and Al_2O_3 in the PTS were reduced to 3.48, 1.54, and 5.85 wt%, respectively. This was due to the high reactivity of the components to form aqueous mineral salts ($CaCl_2$, $MgCl_2$, and $AlCl_3$), and these observations are consistent with the findings of Duan et al. [15], who demonstrated a similar dissolution mechanism during acid leaching of metallurgical slag. Impurity removal is particularly critical for zeolite synthesis, as high concentrations of Ca and Mg are known to hinder the crystallization of ZSM-5 [13]. The resulting beneficiated slag (PTS) exhibited a high amount of SiO_2 (55.23 wt%) and a comparatively low concentration of Al_2O_3 (5.85 wt%). The beneficiation process leached 59.7 % of Al_2O_3, leading to an increase in the Si/Al molar ratio from 2.4 (BFS) to 8.0 (PTS), as detailed in Table 1. While the acid leaching process is beneficial for impurity control, it is essential to maintain a balanced Si/Al ratio to effectively synthesize zeolite frameworks for specific industrial applications.

Anuwattana et al. [16] used acid-leached cupola slag, a waste generated by an iron smelting process, to produce ZSM-5. The initial slag composition, which included SiO_2 (70.1 wt%) and Al_2O_3 (18.9 wt%), was significantly transformed during acid leaching, resulting in a SiO_2-enriched precursor (90.2 wt%) with reduced Al_2O_3 (5.1 wt%), MgO (0.9 wt%), and CaO (2.8 wt%). This substantial reduction in Al_2O_3 (73 %) aligns with findings from Duan et al. [15], who observed a leaching

Table 1
Chemical analysis of BFS and PTS as determined by XRF.

Compound	SiO_2	Al_2O_3	CaO	MgO	Fe_2O_3	MnO	Na_2O	K_2O	TiO_2	P_2O_5	Cr_2O_3	NiO	Si/Al ratio
Blast Furnace Slag (wt%)	40.98	14.51	**29.15**	**8.57**	2.18	0.84	0.25	1.14	0.65	0.02	0.10	0.06	2.4
Pre-treated slag (wt%)	55.23	5.85	**3.48**	**1.54**	0.70	0.03	0.03	0.04	0.90	0.02	0.01	0	8.0

Note: The sum of the chemical compositions does not equal 100 % due to loss on ignition (LOI).

efficiency of 97.3 % (Al_2O_3) whilst investigating the acid-leaching kinetics of blast furnace slag. In their study, the BFS composition showed a lower SiO_2 (34.85 wt%) but significantly higher CaO (42.21 wt%) and MgO (8.42 wt%). The substantial reduction of Al_2O_3 during acid leaching presents a critical challenge for using slag-based precursors in ZSM-5 synthesis, as it disrupts the Si/Al ratio crucial for zeolite framework stability. Conversely, Wajima and Ikegami [17] observed minimum removal of Al_2O_3 (9.54 %) during acid treatment of paper sludge ash. Consequently, the loss of Al_2O_3 during the acid leaching of Si- and Al-rich industrial wastes may be attributed to variations in precursor composition, mineral phase distribution, and reactivity of the waste materials. The reduction of CaO and MgO is essential for enhancing precursor quality in zeolite synthesis, but excessive removal of Al_2O_3 may impede ZSM-5 formation or modify its framework characteristics.

3.2. Diffraction patterns of the synthesized products

Synthesis conditions such as synthesis time and temperature are crucial for controlling the crystallinity and purity of ZSM-5, evidenced by the X-ray diffractograms presented in Fig. 2. Commercial (comm.) ZSM-5 was used as a reference sample, as shown in Fig. 2a and 2b—the characteristic peaks of comm. ZSM-5 are located in the 7.6–8.2° and 22.8–24.5° ranges and were used to establish the presence of ZSM-5 crystals in the synthesized products. In both figures, the diffraction peaks observed at 30° and 36° were identified as residues of the augite mineral [$Ca_{0.74}Fe_{0.087}(Mg_{0.016}Fe_{0.075})(Si_{1.5}Al_{0.5})O_6$] and were observed in all the synthesized products. These peaks were inherited from the pretreated slag, which predominantly consisted of augite as a primary crystalline phase. The XRD pattern of PTS, confirming the presence of augite, has been previously reported by Nyembe et al. (2025). Augite, a crystalline mineral generated by the steel industry, is primarily utilized in the synthesis of polycrystalline composite materials, such as glass ceramics, through heat treatment with nucleating agents [18].

Fig. 2a illustrates the effect of synthesis time on the formation of ZSM-5 at a constant temperature of 180 °C, revealing the critical role of this parameter in controlling the crystallinity of the synthesized product. The product obtained at a crystallization time of 5 h consisted of a broad, narrow, and flat amorphous mineral phase (17.6–26.5°), indicating insignificant framework organization. The ZSM-5 characteristic peaks (7.6–8.2° and 22.8–24.5°) began to form as the synthesis time was increased to 7 h, and the peak intensity increased with an increase in synthesis time to 11 h. At this point, the relative crystallinity was less than 17 %, which implied incomplete crystallization of the amorphous pretreated slag (precursor). A substantial increase in crystallinity was observed at a synthesis time of 13 h, where well-resolved peaks and a relative crystallinity of 52.4 % were achieved, marking this as the favourable synthesis time. Similar trends were reported by Liu et al. [2] during the synthesis of ZSM-5 from natural clay, where significant jump in the relative crystallinity was observed between 3 and 6 h, and well-resolved diffraction peaks were obtained at 7 h, with the crystallinity reaching 88 %. Findings from this study and that of Liu et al. [2] suggest that extending the synthesis time, promotes improved structuring of the ZSM-5 framework, facilitating optimum conditions for nucleation and crystal growth. Therefore, the synthesis time is an essential parameter in controlling the crystallinity of the synthesized ZSM-5.

Fig. 2b illustrates the effect of synthesis temperature on the formation of ZSM-5 at a constant synthesis time of 13 h, highlighting the vital role of temperature in increasing the rate of nucleation and crystal growth during synthesis. The products obtained at lower synthesis temperatures (90, 120, and 150 °C) displayed a prominent amorphous peak (7.2–26.1°) corresponding to an unstructured aluminosilicate mineral phase. The products obtained at higher synthesis temperatures (180 and 200 °C) produced ZSM-5 materials with improved crystallinities (52.4 and 51.2 %, respectively), demonstrating that higher temperatures promote the formation of well-ordered crystalline structures. However, the comparable crystallinities achieved at 180 °C and 200 °C suggest that further increasing the temperature does not significantly enhance ZSM-5 formation, indicating that 180 °C represents a favourable threshold under the current experimental conditions. The increase in crystallinity at higher temperatures was reported by Mohiuddin et al. [10], who attributed it to enhanced nucleation rates and the growth of thermodynamically stable ZSM-5 crystals. Mohiuddin et al. [10] observed that ZSM-5 synthesized from kaolin remained amorphous at 120 °C but formed fully crystalline zeolite phases at 150 °C and 190 °C. This phenomenon, which is also observed in this study, is consistent with

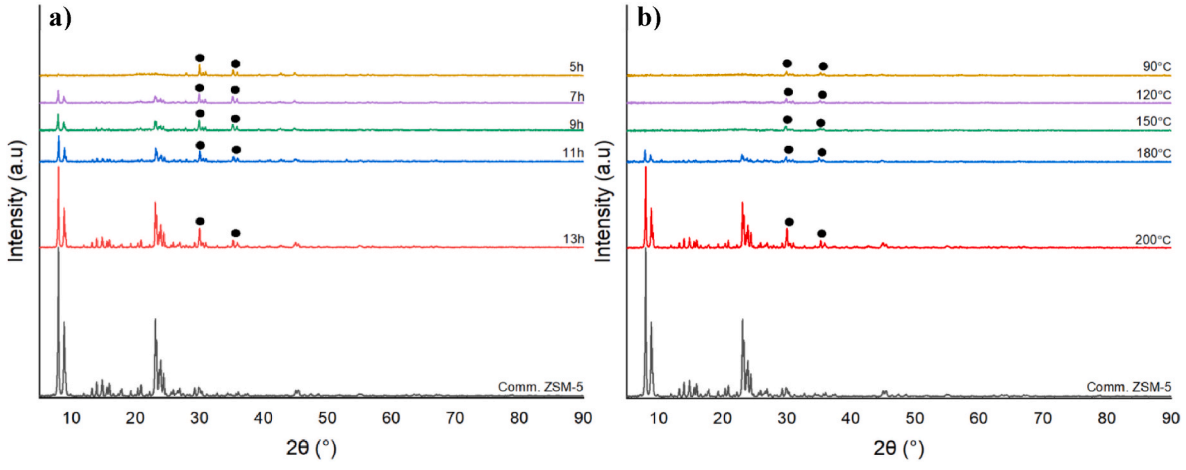

Fig. 2. XRD patterns of the powered samples: a) Effect of synthesis time, b) Effect of synthesis temperature, and (●) Augite mineral.

Ostwald's law of successive reactions, which describes the transformation of metastable phases into more thermodynamically favourable phases under appropriate synthesis conditions [19].

3.3. Morphology of the synthesized products

Fig. 3 shows the crystal morphology and size of the products at different synthesis times, highlighting the progression of crystal refinement and structural development. Commercial ZSM-5 was used as a reference sample and exhibited cubic prism shapes with small intergrown rectangular crystals, demonstrating the ideal morphology. The product obtained after a synthesis time of 5 h consisted of flat, thin sheets stacked to form cubic prisms, indicating the initial stages of nucleation and crystal growth. An increase in the synthesis time to 7 h resulted in the appearance of a morphology similar to that of comm. ZSM-5. However, the surfaces of the crystals were unrefined and surrounded by irregular-shaped particles. At 13 h, the crystals developed into well-defined cubic prisms with microsized intergrown rectangular crystals, closely resembling the reference material. Interestingly, the average crystal size remained constant from 7 to 13 h, suggesting that the primary impact of increased synthesis time was on surface refinement rather than particle size. This is further corroborated by the X-ray diffractograms (Fig. 2), demonstrating that the synthesis time controls the crystallinity of the ZSM-5 framework.

These findings align with Jiang et al. [20], who converted clay mineral waste (palygorskite) into high siliceous ZSM-5 and observed distinct morphological transitions with varying synthesis times. In their study, irregular, spherical, and cubic morphologies were observed at 6, 12, and 24 h, respectively, with no significant change in crystal size beyond 24 h. Similarly, Anuwattana et al. [16] synthesized ZSM-5 from cupola slag and reported the formation of spherical crystals at 12 h, progressing to octagonal prisms with intergrown twin crystals at 20–24 h. These studies highlight a common trend in zeolite synthesis: morphology evolves with synthesis time, transitioning from disordered forms to well-defined crystal structures as nucleation and growth processes mature. Interestingly, the morphologies observed in this study are distinct from those reported by Liu et al. [2], who synthesized ZSM-5 from clay mineral waste (hydromuscovite) and obtained uniform hexagonal plate particles at 7 h. These differences highlight the significant influence of precursor composition on crystal morphology. The constant crystal size observed in this study from 7 to 13 h suggests that the growth of individual crystals stabilizes after a certain point, with further synthesis time primarily enhancing surface refinement.

3.4. Framework structure of synthesized products

The mid-FTIR spectra illustrating the lattice vibration modes of the synthesized products are shown in Fig. 4. Due to the absence of functional groups (>1500 cm^{-1}), the analysis focused on the fingerprint region (1400–400 cm^{-1}). Notably, the silanol (Si–OH) stretching vibrational band, which appears between 3400 and 3600 cm^{-1}, was undetected in all the synthesized products. In Fig. 4a and b, the reference sample (comm. ZSM-5) exhibited well-defined absorption bands at 1224 and 1075 cm^{-1}, characteristic of the external and internal TO_4 (T = Si and Al) asymmetric stretching vibrations, respectively. Moreover, the bands at 798, 546, and 426 cm^{-1} correspond to the internal vibrations of TO_4 symmetric stretching, distorted double five-membered rings, and TO_4 bending, respectively [21]. A sawtooth peak at the low wavenumber range (426 cm^{-1}) was observed in the commercial ZSM-5 but was absent in the experimental samples. This indicates the absence of a highly crystalline and well-ordered aluminosilicate framework in the synthesized products, consistent with their relatively low crystallinity. The presence of such a peak is characteristic of ZSM-5 with fully developed crystalline structures, as observed in previous studies by Krisnandi et al. [22], Jiang et al. [20], and Luo et al. [23]. These structural features confirm the highly ordered aluminosilicate framework characteristic of MFI-type zeolites. The spectra of the synthesized products displayed the typical structural features of comm. ZSM-5 with slight modifications due to the presence of trace metals (Fig. 4a and b). Subtle changes in the spectra, like the appearance of the weak band at 1106 cm^{-1} and differences in band intensity, are attributed to trace metal oxides from the blast furnace slag (BFS) such as Fe_2O_3, MnO, TiO_2, Cr_2O_3, and NiO. These metals can either substitute into the zeolite framework or exist as extra-framework species that may affect their

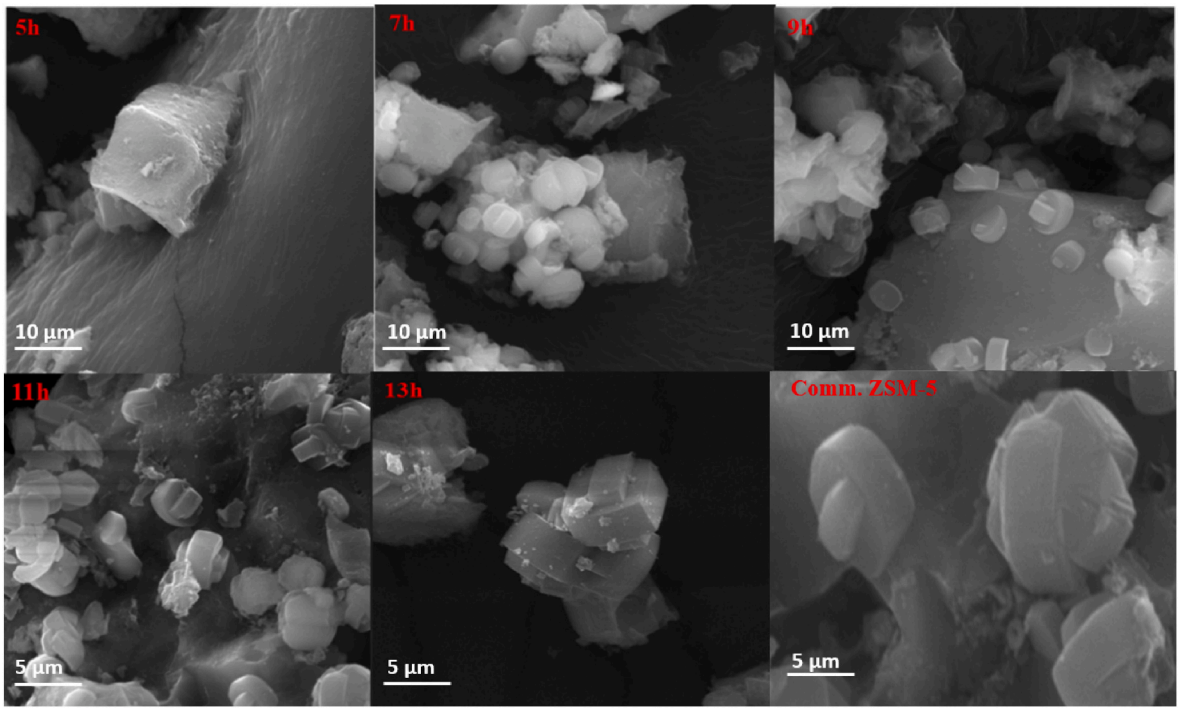

Fig. 3. SEM micro-images of powered samples at different synthesis times.

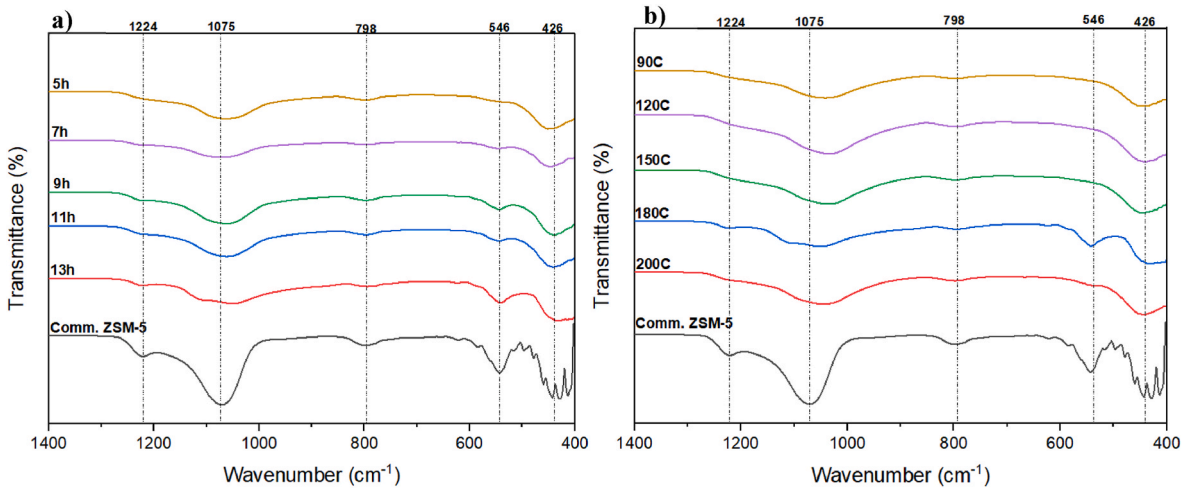

Fig. 4. FT-IT spectra of powdered samples: a) Effect of synthesis time and b) Effect of synthesis temperature.

local structural environment. Previous studies have demonstrated the existence of additional vibrational bands or shifting of existing bands in FTIR spectra of transition metals doped zeolites (either isomorphically or through occlusion), which are due to not only the changes of electron density around the molecule but also the change of bond polarity [24]. To illustrate, the incorporation of Ga^{3+} and Mo^{6+} by Dubray [24] into the tetrahedral framework sites reduced the symmetry and consequently disrupted specific T–O–T bands. Hence, the shifts in FTIR spectra serve as indirect evidence of the presence of trace metals in the zeolite framework and its possible impact on the structural and chemical environment of zeolites.

Synthesis time and temperature had a noticeable effect on the spectra of the synthesized products. That is, products obtained at shorter times (5 h, 7 h) and lower temperatures (90 °C, 120 °C, and 150 °C) lacked the vibration band at 1224 cm^{-1}. This indicates the lack of crystallization to form ZSM-5 crystals [20]. Furthermore, the absence of the vibration band at 546 cm^{-1} for the following products (5 h, 7 h, 90 °C, 120 °C, and 150 °C) further confirms the incomplete crystalline structure. The lack of 1224 and 546 cm^{-1} vibrational bands, supported by their respective diffraction patterns, suggests that these conditions are inadequate to achieve the formation of the ZSM-5 framework. These findings align with Ali et al. [25], who reported that the 1220 and 1090 cm^{-1} bands signify the formation of ZSM-5 crystals and the presence of 3D pores. Comparisons with previous studies further validate these findings, where Wang et al. [26], Luo et al. [23], and Mohiuddin et al. [10] reported double five-ring absorption bands at 546, 542, and 547 cm^{-1}, respectively, which are associated with the three-dimensional pore structure of the ZSM-5 framework. However, in the current study, the synthesized products at shorter times (5 h, 7 h) and lower temperatures (90 °C, 120 °C, and 150 °C) did not exhibit a well-defined band at 546 cm^{-1}, emphasizing incomplete crystallization at these conditions. Moreover, the molecular structure of ZSM-5 can be identified and verified using the infrared (IR) optical density ratio. This is done by computing the area ratio of the vibrational bands at 426 and 546 cm^{-1}. An ideal ZSM-5 zeolite typically exhibits an optical density ratio of approximately 0.72 [27]. In this study, the reference ZSM-5 displayed a slightly lower optical density ratio of 0.67, indicating minor structural variations, while the synthesized products lacked sufficient crystallinity to determine these values.

3.5. Texture properties of the synthesized products

Table 2 presents the specific surface area and porosity characteristics of the synthesized ZSM-5 samples focusing only on the products that displayed distinctive diffraction profiles (Fig. 2) unique to ZSM-5. The reference sample contained an average pore size and specific surface area of 2.62 nm and 436.4 m^2/g, respectively. This shows a micro- and mesoporous structure, as noted by the micropore volume (0.105 cm^3/g), further confirmed by the sorption isotherm in Fig. 5, highlighting its high crystallinity and well-defined pore framework. In contrast, the synthesized ZSM-5 products displayed significantly larger pore sizes and lower specific surface areas. For instance, an increase in synthesis time (from 9 to 13 h) decreased the average pore size from 70.6 to 14.8 nm, suggesting that extended synthesis time promotes the development of

Table 2
Textural and structural properties of the powdered samples.

Sample	S_{BET} (m^2/g)	V_{tot} (cm^3/g)	V_{micro} (cm^3/g)	Pore diameter (nm)	Crystallinity (%)	Si/Al molar ratio
Comm. ZSM-5	436.4	0.286	0.105	2.62	100	25
13 h	108.4	0.394	n.d.	14.8	52.4	11.9
11 h	106.6	0.448	n.d.	16.5	16.9	11.9
9 h	95.7	0.169	n.d.	70.6	12.7	11.9
200 °C	104.6	0.403	n.d.	24.9	51.2	11.9

n.d. = not detected.

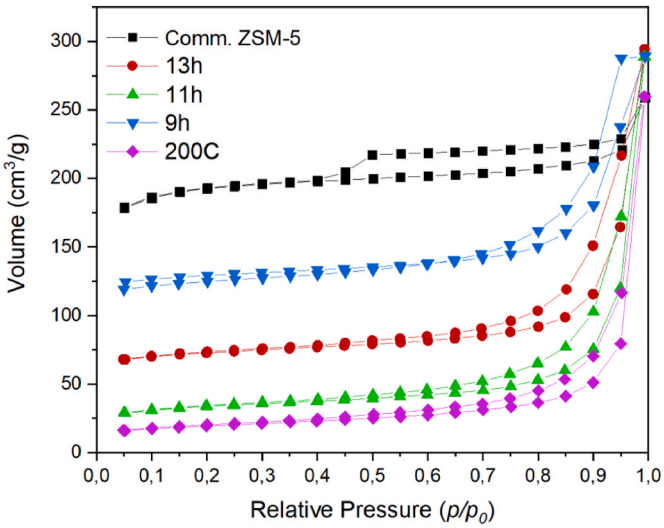

Fig. 5. Nitrogen sorption isotherms of powdered samples.

smaller pores and more refined structures. The synthesized ZSM-5 products comprised mesopores, whereas the product at 9 h comprised macropores (70.6 nm). The specific surface area and crystallinity of the synthesized ZSM-5 products were relatively low due to the trace metals deposited onto the mesopores, as supported by the FT-IR spectra (Fig. 4).

Overall, the low crystallinity achieved by the synthesized ZSM-5 products displayed incomplete crystallization [28]; however, the highest relative crystallinity was 52.4 % (13 h). The crystallinity values obtained at 200 °C (51.2 %) and 180 °C (52.4 %) are within the acceptable error range of ±5 %. The Si/Al molar ratio was constant for all synthesized ZSM-5 products, indicating that the variations in the synthesis time and temperature do not affect the chemical composition of the products (Table 2). Although the synthesized ZSM-5 products contained trace metals such as Fe, Mn, Cr, Ti, and Ni, their relatively low concentrations did not significantly impact the measured bulk Si/Al ratios. However, their presence may induce minor structural distortions, lead to pore blocking, or promote mesopore enhancement; ultimately affecting the surface area and pore size distribution. Even though no direct quantification of these effects was performed in the present work, it has been previously observed that these types of metal substitution impact the physicochemical properties of zeolites [24]. Comparisons with existing studies reveal the limitations of the current synthesis method. For instance, Jiang et al. [20] reported that the increased synthesis time (6–120 h) significantly improved the specific surface area from 50 to 271 m^2/g. Similarly, Krisnandi et al. [22] achieved a surface area of 294.75 m^2/g for ZSM-5 synthesized from rice husk ash (144 h), Wu et al. [29] obtained 263 m^2/g from a fibrous clay mineral (48 h), and Zhou et al. [30] reported 339 m^2/g using a clay mineral (12 h). These results emphasize the role of synthesis time, temperature, and precursor selection on the textural properties of the final product. Despite the relatively low surface area of the synthesized products, the presence of mesopores may offer unique advantages for specific applications, such as adsorption or catalysis, where a combination of micro- and mesoporosity is desirable.

Fig. 5 shows the nitrogen physisorption isotherms and hysteresis curves of the synthesized ZSM-5 products, providing valuable insights into their porosity dynamics. It can be observed that none of the products exhibited a sharp increase in adsorption at a relative pressure of $10^{-6} < p/p_0 < 0.01$. This is due to the absence of a microporous structure in all the products [2]. Instead, all the powdered samples displayed a type-IV adsorption isotherm with distinct hysteresis loops characteristic of capillary condensation occurring at high relative pressure, indicating the presence of mesopore structures [31]. The type-IV adsorption isotherm is typically obtained when synthesizing hierarchical ZSM-5 zeolite. The presence of type-IV isotherms in the synthesized products aligns with studies on hierarchical ZSM-5 synthesis, such as Wu et al. [29], who obtained it using fibrous clay to synthesize large mesoporous intracrystals, Nandiwale et al. [32] obtained it using a mesopore structure directing agent, and Popova et al. [28] converted a microporous ZSM-5 to hierarchical ZSM-5 using a mixture of ammonium fluoride and hydrofluoric acid.

These comparisons emphasize that the observed mesoporosity in the synthesized ZSM-5 products reflects their hierarchical structure. In the high relative pressure ($p/p_0 > 0.6$) region, the synthesized ZSM-5 products depicted steep hysteresis loops that differed from the reference sample, suggesting varying mesoporous and macroporous structures. In other words, the products obtained at 13, 11, and 9 h consisted of the type-H1 hysteresis loop, indicative of uniform mesopores with an open geometry in a narrow range [31]. A type-H4 hysteresis loop was observed in the reference sample, which indicates a mesoporous structure with narrow slit-like pores. Lastly, the product obtained at 9 h comprised a type-H2 hysteresis loop, which describes a mesoporous and macroporous distribution of pore sizes and shapes that are not well-defined [33]. These varying hysteresis loops observed in the powered samples further reveal distinctions in pore geometry and distribution.

3.6. Chemical composition of ZSM-5

Table 3 compares the chemical composition of the synthesized ZSM-5 to the reference sample, providing insights into the influence of pretreated slag and synthesis conditions. The synthesized ZSM-5 was selected based on the favourable synthesis conditions, which were 13 h and 180 °C. Both porous materials consisted mainly of SiO_2 and less Al_2O_3, affirming their classification as high-silica zeolites (Si/Al > 5). Interestingly, the chemical composition of the synthesized ZSM-5 was found to be unaffected by variations in synthesis temperature and time, as evidenced by the constant Si/Al molar ratio in Table 2. The Si/Al ratio of commercial ZSM-5 was observed to be twice that of synthesized ZSM-5, indicating differences in framework composition. The transition in Si/Al ratio from the pretreated slag (8.0; Table 1) to the synthesized ZSM-5 (11.9; Table 3) suggests that the synthesis process favored the incorporation of more silicon relative to aluminum. This phenomenon likely occurred during stages such as the dissolution of Si and Al components, generation of reactive species, formation of ZSM-5 building blocks, and eventual crystal growth [34]. It is within these stages that factors such as preferential silicon integration, aluminum dissolution, or the emergence of secondary phases may impact the Si/Al ratio of ZSM-5.

The synthesized ZSM-5 contained impurities such as CaO (5.34 wt %), MgO (2.36 wt%), and trace metals (11.63 wt%), and this was due to the starting material used (blast furnace slag) during synthesis. While the presence of impurities has shown the challenges of utilizing blast furnace slag as feedstock, the presence of trace metals could improve the catalytic reactivity of the material, introducing opportunities for functional enhancement. That is, transitional metals such as Cr_2O_3, MnO, and Fe_2O_3 have demonstrated improved catalytic activity of ZSM-5 in applications such as environmental remediation or petrochemical catalysis. For instance, Wang et al. [35] impregnated ZSM-5 with copper and manganese to improve its adsorptive properties and reduce the oxides of nitrogen from the atmosphere. In another study, Chiosso et al. [36] dopped Zn, Cr, and Fe to modify the properties of hierarchal ZSM-5 for the catalytic cracking of bio-oil. Therefore, the inherent presence of trace metals in the current study offers a unique advantage of eliminating additional doping steps required to modify commercial ZSM-5, thus potentially reducing processing costs. However, future research should focus on assessing the impact of inherent trace metals on petrochemical reaction performance.

4. Conclusion

The study successfully integrated green chemistry principles with the hydrothermal synthesis technique to enhance the production of a novel ZSM-5 zeolite. By utilizing blast furnace slag as a silica and alumina source, along with microwave irradiation for energy-efficient heating, impurities such as CaO and MgO were significantly reduced, further enhancing the sustainability of the process. The resulting ZSM-5 displayed a moderate crystalline phase, characterized by distinct micro-sized intergrown rectangular crystals similar to the commercial ZSM-5. Notably, the crystalline morphology of the synthesized ZSM-5 was found to be significantly influenced by synthesis conditions, with synthesis time playing a key role in surface refinement and temperature affecting crystal size. In comparison, the commercial ZSM-5 exhibited a micro-

Table 3
Metal composition of ZSM-5.

Compound	SiO_2	Al_2O_3	CaO	MgO	Traces	Si/Al ratio
Synthesized ZSM-5 (wt %)	75.29	5.38	5.34	2.36	11.63	**11.9**
Commercial ZSM-5 (wt %)	96.67	3.28	0	0	0.05	**25.0**

Traces: Fe_2O_3, MnO, Na_2O, K_2O, TiO_2, P_2O_5, Cr_2O_3 and NiO.

mesoporous nature with a high specific surface area, while the synthesized counterpart showcased a mesoporous crystalline structure with a relatively lower specific surface area. Ultimately, the favourable synthesis conditions were determined to be 13 h and 180 °C, yielding a high-silica ZSM-5 product with a stable Si/Al molar ratio that remained unaffected by variations in temperature or time. This underscores the reliability of using BFS as an industrial hazardous waste in the production of ZSM-5 zeolite. Overall, this study highlights the feasibility of valorizing metallurgical waste for advanced material synthesis, contributing to the circular economy and promoting sustainable practices in zeolite production. Future work could focus on the application of the synthesized ZSM-5 in catalyzing petrochemical reactions whilst evaluating the catalyst's structural and textural characteristics, as well as the influence of trace metals.

Author contributions

Nhlanhla Nyembe: Data curation; formal analysis; investigation; methodology; validation; writing – original draft; writing – review and editing.

Yusuf Isa: Conceptualization; methodology; project administration; resources; supervision; validation; writing – review and editing.

Declaration of competing interest

The authors declare that they have no known competing financial interests or personal relationships that could have appeared to influence the work reported in this paper.

Acknowledgements

The authors would like to acknowledge the full support of the Petrochemical and Fuels Synthesis group and the University of Witwatersrand.

Data availability

Data will be made available on request.

References

[1] J. Grams, A.M. Ruppert, Catalyst stability—bottleneck of efficient catalytic pyrolysis, in: Catalysts, 11, 2021, pp. 1–24, https://doi.org/10.3390/catal11020265 (2),MDPI.
[2] Y. Liu, S. Han, D. Guan, S. Chen, Y. Wu, Y. Yang, N. Jiang, Rapid green synthesis of ZSM-5 zeolite from leached illite clay, Microporous Mesoporous Mater. 280 (2019) 324–330, https://doi.org/10.1016/j.micromeso.2019.02.027.
[3] B. Jha, D.N. Singh, A review on synthesis, characterization and industrial applications of Flyash zeolites, J. Mater. Educ. 33 (1–2) (2011) 65–132.
[4] S. Wang, X. Jiang, G. Nie, Z. Wang, H. Yu, Y. Liu, Q. Wu, S. Yu, S. Liu, Trash into treasure: nano ZSM-5 catalyst for cracking waste cooking oil to bio-gasoline with enhanced selectivity, Fuel Process. Technol. 242 (2023) 107666, https://doi.org/10.1016/j.fuproc.2023.107666.
[5] H. Zhang, I. bin Samsudin, S. Jaenicke, G.K. Chuah, Zeolites in catalysis: sustainable synthesis and its impact on properties and applications, Catal. Sci. Technol. 12 (19) (2022) 6024–6039, https://doi.org/10.1039/D2CY01325H.
[6] E.R. Parnham, R.E. Morris, The ionothermal synthesis of cobalt aluminophosphate zeolite frameworks, J. Am. Chem. Soc. 128 (7) (2006) 2204–2205, https://doi.org/10.1021/JA057933L/SUPPL_FILE/JA057933LSI20051122_094614.CIF.
[7] X. Meng, F.S. Xiao, Green routes for synthesis of zeolites, Chem. Rev. 114 (2) (2014) 1521–1543, https://doi.org/10.1021/cr4001513.
[8] S. Han, Y. Liu, C. Yin, N. Jiang, Fast synthesis of submicron ZSM-5 zeolite from leached illite clay using a seed-assisted method, Microporous Mesoporous Mater. 275 (2019) 223–228, https://doi.org/10.1016/j.micromeso.2018.08.028.
[9] Q. Wu, X. Wang, G. Qi, Q. Guo, S. Pan, X. Meng, J. Xu, F. Deng, F. Fan, Z. Feng, C. Li, S. Maurer, U. Müller, F.S. Xiao, Sustainable synthesis of zeolites without addition of both organotemplates and solvents, J. Am. Chem. Soc. 136 (10) (2014) 4019–4025, https://doi.org/10.1021/ja500098j.
[10] E. Mohiuddin, Y.M. Isa, M.M. Mdleleni, N. Sincadu, D. Key, T. Tshabalala, Synthesis of ZSM-5 from impure and beneficiated Grahamstown kaolin: effect of kaolinite content, crystallisation temperatures and time, Appl. Clay Sci. 119 (2016) 213–221, https://doi.org/10.1016/j.clay.2015.10.008.
[11] H.M. Morgan, Q. Bu, J. Liang, Y. Liu, H. Mao, A. Shi, H. Lei, R. Ruan, A review of catalytic microwave pyrolysis of lignocellulosic biomass for value-added fuel and chemicals, Bioresour. Technol. 230 (2017) 112–121, https://doi.org/10.1016/j.biortech.2017.01.059.
[12] A. Kumar, Y. Kuang, Z. Liang, X. Sun, Microwave chemistry, recent advancements, and eco-friendly microwave-assisted synthesis of nanoarchitectures and their applications: a review, Materials Today Nano 11 (2020) 100076, https://doi.org/10.1016/J.MTNANO.2020.100076.
[13] N. Nyembe, Y.M. Isa, Acid leaching of blast furnace slag for enhanced zeolite synthesis, Cleaner Waste Systems 10 (2025) 100207, https://doi.org/10.1016/j.clwas.2025.100207.
[14] J. Gu, Y. Jin, Y. Zhou, M. Zhang, Y. Wu, J. Wang, Unseeded organotemplate-free hydrothermal synthesis of heteroatomic MFI zeolite poly-nanocrystallites, J. Mater. Chem. A 1 (7) (2013) 2453–2460, https://doi.org/10.1039/c2ta01009g.
[15] W. Duan, D. Wang, Z. Wang, Q. Yu, Hydrometallurgical leaching behavior and kinetic modeling of blast furnace slag in hydrochloric acid, Journal of Sustainable Metallurgy 8 (1) (2022) 170–185, https://doi.org/10.1007/s40831-021-00473-w.
[16] R. Anuwattana, K.J. Balkus, S. Asavapisit, P. Khummongkol, Conventional and microwave hydrothermal synthesis of zeolite ZSM-5 from the cupola slag, Microporous Mesoporous Mater. 111 (1–3) (2008) 260–266, https://doi.org/10.1016/j.micromeso.2007.07.039.
[17] T. Wajima, Y. Ikegami, Zeolite synthesis from paper sludge ash via acid leaching, Chem. Eng. Commun. 195 (3) (2008) 305–315, https://doi.org/10.1080/00986440701555258.
[18] L. Deng, F. Yun, R. Jia, H. Li, X. Jia, Y. Shi, X. Zhang, Effect of SiO2/MgO ratio on the crystallization behavior, structure, and properties of wollastonite-augite glass-ceramics derived from stainless steel slag, Mater. Chem. Phys. 239 (2020) 122039, https://doi.org/10.1016/J.MATCHEMPHYS.2019.122039.
[19] E. Mohiuddin, Y.M. Isa, M.M. Mdleleni, D. Key, Synthesis and application of porous kaolin-based ZSM-5 in the petrochemical industry, Nanofluid Flow in Porous Media (2018) 1–26, https://doi.org/10.5772/intechopen.77588.
[20] J. Jiang, C. Duanmu, Y. Yang, X. Gu, J. Chen, Synthesis and characterization of high siliceous ZSM-5 zeolite from acid-treated palygorskite, Powder Technol. 251 (2014) 9–14, https://doi.org/10.1016/j.powtec.2013.10.020.
[21] R.K. Ahedi, A.N. Kotasthane, B.S. Rao, A. Manna, B.D. Kulkarni, Synthesis of ferrierite-type zeolite in the presence of a catalytic amount of pyrrolidine and sodium bis(2-ethyhlhexyl) sulfosuccinate, J. Colloid Interface Sci. 236 (1) (2001) 47–51, https://doi.org/10.1006/jcis.2000.7390.
[22] Y.K. Krisnandi, F.M. Yanti, S.D.S. Murti, Synthesis of ZSM-5 zeolite from coal fly ash and rice husk: characterization and application for partial oxidation of methane to methanol, in: IOP Conference Series: Materials Science and Engineering, 188, 2018 012031, https://doi.org/10.1088/1742-6596/755/1/011001.
[23] W. Luo, X. Yang, Z. Wang, W. Huang, J. Chen, W. Jiang, L. Wang, X. Cheng, Y. Deng, D. Zhao, Synthesis of ZSM-5 aggregates made of zeolite nanocrystals through a simple solvent-free method, Microporous Mesoporous Mater. 243 (2017) 112–118, https://doi.org/10.1016/j.micromeso.2017.01.040.
[24] F. Dubray, Incorporation of Metals in Zeolite Frameworks for Catalytic Applications, 1, Normandie Université, Organic Chemistry, Normandy, 2020, pp. 1–165 [PhD Thesis], https://doi.org/theses.hal.science/tel-03510144. Accessed 8 April 2025.
[25] I. Ali, A. Hassan, S. Shabaan, K. El-Nasser, Synthesis and characterization of composite catalysts Cr/ZSM-5 and their effects toward photocatalytic degradation of p-nitrophenol, Arab. J. Chem. 10 (2017) S2106–S2114, https://doi.org/10.1016/j.arabjc.2013.07.042.
[26] P. Wang, B. Shen, J. Gao, Synthesis of ZSM-5 zeolite from expanded perlite and its catalytic performance in FCC gasoline aromatization, Catal. Today 125 (3–4) (2007) 155–162, https://doi.org/10.1016/j.cattod.2007.03.010.
[27] D.J. Kim, H.S. Chung, Synthesis and characterization of ZSM-5 zeolite from serpentine, Appl. Clay Sci. 24 (1–2) (2003) 69–77, https://doi.org/10.1016/S0169-1317(03)00149-2.
[28] M. Popova, Á. Szegedi, M. Oykova, H. Lazarova, N. Koseva, M.R. Mihályi, P. Shestakova, Selective production of phenol on bifunctional, hierarchical zsm-5 zeolites, Molecules 26 (12) (2021), https://doi.org/10.3390/molecules26123576.
[29] M. Wu, W. Jiang, J. Jiang, Y. Zou, P. Zhang, P. Mao, Y. Xu, Y. Shi, Synthesis of ZSM-5 zeolites using palygorskite as raw material under solvent-free conditions, Bull. Mater. Sci. 43 (2020) 289, https://doi.org/10.1007/s12034-020-02263-8S.
[30] X. Zhou, Y. Liu, X. Meng, B. Shen, F. Xiao, Synthesis and catalytic cracking performance of Fe/Ti-ZSM-5 zeolite from attapulgite mineral, Cuihua Xuebao/Chinese Journal of Catalysis 34 (8) (2013) 1504–1512, https://doi.org/10.1016/S1872-2067(12)60638-X.
[31] B. Liu, L. Zheng, Z. Zhu, K. Zhang, H. Xi, Y. Qian, Effect of synthesis conditions on the structural and catalytic properties of hierarchically structured ZSM-5 zeolites, RSC Adv. 4 (27) (2014) 13831–13838, https://doi.org/10.1039/C4RA00124A.
[32] K.Y. Nandiwale, A.M. Pande, V.V. Bokade, One step synthesis of ethyl levulinate biofuel by ethanolysis of renewable furfuryl alcohol over hierarchical zeolite catalyst, RSC Adv. 5 (97) (2015) 79224–79231, https://doi.org/10.1039/c5ra13520f.
[33] K.S.W. Sing, D.H. Everett, R.A.W. Haul, L. Moscou, R.A. Pierotti, J. Rouquerol, T. Siemieniewska, Reporting physisorption data for gas/solid systems-with special reference to the determination of surface area and porosity, Pure Appl. Chem. 57 (4) (1985) 603–619.

[34] C. Liu, D. Kong, H. Guo, The morphology control of zeolite ZSM-5 by regulating the polymerization degree of silicon and aluminum sources, Microporous Mesoporous Mater. 193 (2014) 61–68, https://doi.org/10.1016/j.micromeso.2014.03.015.
[35] T. Wang, X. Zhang, J. Liu, H. Liu, Y. Wang, B. Sun, Effects of temperature on NOx removal with Mn-Cu/ZSM5 catalysts assisted by plasma, Appl. Therm. Eng. 130 (2018) 1224–1232, https://doi.org/10.1016/J.APPLTHERMALENG.2017.11.113.
[36] M.E. Chiosso, I. Crespo, A.B. Merlo, B. Valle, Metal-doped HZSM-5 zeolite catalysts for catalytic cracking of raw bio-oil: exploring activity toward value-added products, Catalysts 13 (8) (2023) 1198, https://doi.org/10.3390/CATAL13081198. *Page 1198*, 13.